

Neutron tunneling: A new mechanism to power explosive phenomena in neutron stars, magnetars, and neutron star mergers

CARLOS A. BERTULANI¹ AND RONALDO V. LOBATO¹

¹*Department of Physics and Astronomy, Texas A&M University-Commerce, Commerce, TX 75429, USA*

(Dated: June 28, 2022)

ABSTRACT

Neutron tunneling between neutron-rich nuclei in inhomogeneous dense matter encountered in neutron star crusts can release enormous energy on a short-timescale to power explosive phenomena in neutron stars. In this work we clarify aspects of this process that can occur in the outer regions of neutron stars when oscillations or cataclysmic events increase the ambient density. We use a time-dependent Hartree-Fock-Bogoliubov formalism to determine the rate of neutron diffusion and find that large amounts of energy can be released rapidly. The role of nuclear binding, the two-body interaction and pairing, on the neutron diffusion times is investigated. We consider a one-dimensional quantum diffusion model and extend our analysis to study the impact of diffusion in three-dimensions. We find that these novel neutron transfer reactions can generate energy at the amount of $\simeq 10^{40} - 10^{44}$ ergs under suitable conditions.

1. INTRODUCTION

Diffusion is a quantitative physical exchange of particles in environments with inhomogeneous particle spatial distribution. In nuclear physics it has been studied in central collisions between heavy ions due to a momentarily local imbalance of protons and neutrons (Tsang et al. 2004). The goal in such studies is to understand the contribution of the symmetry energy term to the equation of state of neutron stars (Shi & Danielewicz 2003). Energy and isospin imbalance also occurs in the crust of neutron stars where dense neutron regions coexist with neutron poorer regions. In a non-equilibrated environment, neutrons will diffuse to lower the energy leading to a near homogenization of the neutron density. Neutron transfer can also occur between isospin unbalanced nuclear processes that could modify the cooling rates in transiently accreting neutron stars (Chugunov 2018). Neutron transfer, or diffusion, in neutron star mergers will also influence the rate at which a locally homogeneous density can be achieved. Clumps and voids are certainly formed during the merging process and/or during a fallback mechanism in a core-collapse supernovae. Supernova fallback accretion has been intensively studied as possible site for r-process (Fryer et al. 2006) and as source of long-duration gamma-ray bursts in newly formed magnetars (Piro & Ott 2011; Metzger et al. 2018).

In this work we explore the physics of diffusion in inhomogeneous neutron media due to tunneling, considering the flow of individual neutrons as well as neutron-pairs through the nuclear mean-field. For simplicity, we assume charge-neutral systems, i.e., pure neutron matter. Our goal is to identify general features and possible scaling laws for the diffusion rates that can be used to estimate cooling properties of neutron stars, and homogenization lifetimes in their crusts. We propose that the fast tunneling times of loosely bound neutrons can trigger short gamma/X-ray bursts/flaring activities in magnetars and fast radio burst (FRBs) through the liberation of photons in the crust or in the star magnetic field. Beta decay particles in the strong magnetic field move perpendicular to it in quantized Landau levels and the electron-cyclotron energy will be equal to the electron rest-mass energy. In this scenario these particles will also act as a seed for the high energy electromagnetic radiation. The origin of these electromagnetic activities as well as the sources of the FRBs are unknown. Recent observations have shown a connection between these phenomena (Lin et al. 2020; Bochenek et al. 2020a; Andersen et al. 2020), maybe solving the puzzling mechanism of FRBs sources.

Corresponding author:

carlos.bertulani@tamuc.edu, ronaldo.lobato@tamuc.edu

First, we study a one-dimensional system where a neutron dense region has at least two neighboring uncompressed regions. One dimensional models, such as the 1D Ising model, have fundamentally impacted our knowledge of thermodynamics, critical phenomena, particle physics, conformal quantum field theories, magnetism, and emergence in many-body systems. The existence of two neighbors enhances the equilibration rates, and in three-dimensions this enhancement will increase appreciably. Because of resonant tunneling, neutrons diffuse primarily to states with approximately the same single-particle energies followed by decay to states at lower energies or by other nuclear processes such as beta-decay or gamma emission. Transfer of loosely-bound neutrons and the presence of neighbors leads to neutron diffusion estimates that deviate considerably from the well-known WKB approximation. As expected, the neutron-neutron interaction and pairing are important effects not treatable under perturbation theory.

2. HFB DIFFUSION MODEL.

We consider the dynamics of a one dimensional system of neutrons in a one-body potential $U(x)$ and a neutron-neutron interaction $v(x, x')$ solving the Time-Dependent Hartree-Fock-Bogoliubov (TDHFB) equations (Ring & Schuck 1980)

$$i\hbar \frac{\partial}{\partial t} u_\alpha(x, t) = \left\{ -\frac{\hbar^2 \Delta_x^{(2)}}{2m(\delta x)^2} + U(x) + \Gamma(x) \right\} u_\alpha(x, t) - \delta x \sum_{x'} \Delta(x, x') v_\alpha(x', t) \quad (1a)$$

$$i\hbar \frac{\partial}{\partial t} v_\alpha(x, t) = - \left\{ -\frac{\hbar^2 \Delta_x^{(2)}}{2m(\delta x)^2} + U(x) + \Gamma^*(x) \right\} v_\alpha(x, t) - \delta x \sum_{x'} \Delta^*(x, x') u_\alpha(x', t), \quad (1b)$$

where $\hbar^2/2m = 20.73 \text{ MeV fm}^2$, $|u_\alpha|^2$ ($|v_\alpha|^2$) represents the probability that a pair state α is occupied (unoccupied), δx is the size step of a discretized one-dimensional mesh, and $\Delta_x^{(2)}$ is the second-order differential operator $\Delta_x^{(2)}\phi(x) = \phi(x + \delta x) - 2\phi(x) + \phi(x - \delta x)$. The other quantities are defined as

$$\Gamma(x) = \sum_{x'} v(x - x') \rho(x', x') \quad (2)$$

$$\Delta(x, x') = v(x - x') \kappa(x, x') \quad (3)$$

$$\rho(x, x') = \sum_{\alpha} v_\alpha^*(x, t) v_\alpha(x', t) \quad (4)$$

$$\kappa(x, x') = \sum_{\alpha} v_\alpha^*(x, t) u_\alpha(x', t), \quad (5)$$

where $\rho(x, x')$ is the density matrix, $\kappa(x, x')$ is the pairing density matrix, $\Delta(x, x')$ is the pair correlation matrix, and $\Gamma(x)$ is the interaction density. These time-dependent coupled-equations are solved with a fourth-order classical Runge-Kutta method.

The initial ($t = 0$) wavefunction is obtained by diagonalizing the standard Hartree-Fock-Bogoliubov (HFB) equations using an expansion of single-particle states in a harmonic oscillator basis with particle-number conservation enforced with the Lagrange multiplier method (Ring & Schuck 1980). This model yields the initial states α and their energies and occupation numbers for a system of N neutrons. We assume spin symmetry, so that $u_{\alpha\uparrow} = u_{\alpha\downarrow}$ ($v_{\alpha\uparrow} = v_{\alpha\downarrow}$) which reduces the working model space to half the number of states needed.

We consider initially neutron clumps of typical nuclear sizes using a confining potential $U_{t=0}(x) = U(x) + U_\lambda(x)$ with

$$U(x) = \frac{U_0}{[1 + \exp\{|x| - d\}/a]}, \quad (6)$$

and parameters, $U_0 = -100 \text{ MeV}$, $d = 5 \text{ fm}$ and $a = 1 \text{ fm}$. For the neutron-neutron potential we assume a Gaussian interaction of the form

$$v(x, x') = v_0 \exp\left(-\frac{|x - x'|^2}{2\sigma_0^2}\right), \quad (7)$$

with $v_0 = -14$ MeV and $\sigma_0 = 2.5$ fm. To simulate loosely-bound neutrons and obtain the chemical potential close to the continuum, we add to $U(x)$ at $t = 0$ a confining harmonic oscillator potential $U_\lambda(x) = \lambda x^2$ and use λ as a parameter to adjust the binding energy of the system.

For $N = 20, 40, 80$ and 160 neutrons, with $\lambda = 2, 10^{-1}, 1.15 \times 10^{-2}$, and 2×10^{-3} MeV/fm $^{-2}$, and the potential parameters for $U(x)$ and $v(x, x')$ as listed above, the solution of the static HFB equations yields valence neutrons bound by $S_n = 1.55, 0.96, 0.40$, and 0.25 MeV for $N = 20, 40, 80$ and 160 neutrons, respectively, where S_n denotes the neutron separation energy. This is displayed in Table 1 together with other energies in the system. The binding energies per neutron are much larger than for a regular nuclear system, however the physics associated with the diffusion rate of the neutrons can be well understood with this model.

N	λ [MeV/fm $^{-2}$]	$E_{s.p.}$	E_{kin}	E_{int}	E_{pair}	E_{total}	S_n
20	2	-1353	767.9	-690.4	-6.72	-1282	1.55
40	0.1	-1830	1384	-1457	-4.97	-1908	0.96
80	1.15×10^{-2}	-1812	2222	-2550	-7.27	-2146	0.40
160	2.0×10^{-3}	-1610	3632	-4466	-12.3	-2456	0.25

Table 1. Single particle energy, $E_{s.p.}$, kinetic energy, E_{kin} , interaction energy, E_{int} , pairing energy, E_{pair} , total energy, E_{total} and neutron separation energy, S_n , for a system of $N = 20, 40, 80$ and 160 neutrons confined in a potential with parameters described in text. All energies are in units of MeV.

3. TIME EVOLUTION AND DIFFUSION RATES.

After the preparation of the initial wavefunction for N neutrons, we solve Eqs. (1) switching-off the confining potential U_λ . The potential $U(x)$ as described above, is replaced by a chain of equally-shaped Woods-Saxon-type potentials separated by a distance D . Namely, at $t > 0$ we make the replacement

$$U(x, d, a) \rightarrow \sum_{n=-M}^M U(x - nD, d, a). \quad (8)$$

The initial wavefunction, as described previously, is located at the center of the potential chain, i.e., for the term of the sum with $n = 0$. The N -neutron system is thus allowed to evolve with the neutrons tunneling through the barriers with equal widths of about $D - 2(d + a)$. The Eqs. (1) are solved within a box of size $L = 100$ fm, and absorbing boundary conditions with an imaginary potential, located at the edges of the box, with thickness $d_{im} = 50$ fm and strength $W_{im} = -200$ MeV. The absorbing boundary conditions avoid reflections at the borders of the box, relevant for large time scales. The number $2M$ of potential wells entering Eq. (8) depends on the distance D between them. Initially, we use $M = 2 - 10$ for D in the range $D = 20 - 100$.

The N -neutron wavefunction is allowed to evolve and the diffusion from the dense to the uncompressed regions predominantly occurs for the neutrons with the smallest separation energies. Tunneling to neighboring clumps will be partially Pauli-blocked preventing neutrons to flow (Ogata & Bertulani 2020). Therefore, valence neutrons will be freer to move between the potential pockets and our model captures the relevant aspects of the diffusion process.

The time evolution of the neutron density enable us to calculate the neutron diffusion speed and the net diffusion coefficient \mathcal{D} by using the equation $\partial \langle \rho \rangle / \partial t = \mathcal{D} \partial^2 \langle \rho \rangle / \partial x^2$. In our 1D model we assess the rate at which the neutrons diffuse from a dense to an uncompressed region by calculating the neutron transfer rate $\Lambda_n(t)$ from $\Lambda_n(t) = -dN_0/dt$ where $N_0(t)$ is the number of neutrons confined within the initial neutron clump centered at $x = 0$ corresponding to $n = 0$ in Eq. (8).

Alternatively, the tunneling rate can be calculated using Gamow's model for nuclear decay (Gamow 1928)

$$\begin{aligned} \Lambda_G &= \nu P \sim \frac{v}{d} \exp \left(-2 \int |\kappa(x)| dx \right) \\ &\sim \frac{\sqrt{2U_0/m}}{d} \exp \left(-\frac{2}{\hbar} \int \sqrt{2m[U(x) - E]} dx \right), \end{aligned} \quad (9)$$

where $\nu \sim v/d$ is the barrier assault frequency and $\hbar\kappa = \sqrt{2m[U(x) - E]}$ is the local momentum for a particle with kinetic energy E . The integral is performed between the turning points where $E = U(x)$. For the most energetic

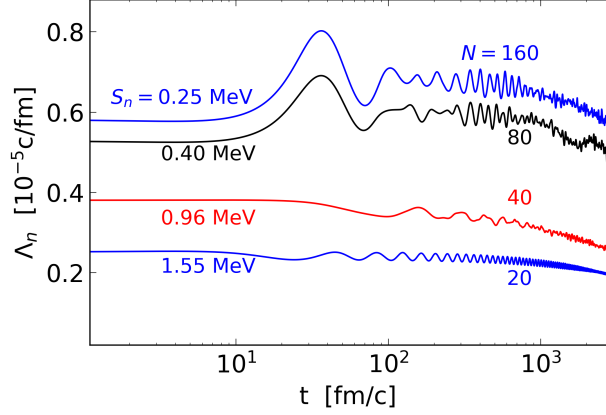


Figure 1. Neutron diffusion rates as a function of time for the neutron clumps separated by 20 fm with neutron numbers listed in Table 1 and a periodic row of Woods-Saxon potentials as described in the text.

neutrons, i.e., the ones occupying the last orbital for the cases listed in Table 1, we have $v \sim \sqrt{2U_0/m}$ and the Gamow model yields increasing tunneling rates $\Lambda_G \sim (0.5 - 0.9) \times 10^{-5}$ c/fm for decreasing separation energies $S_n = (1.55 - 0.25)$ MeV.

As shown in Figure 1, the neutron transfer rates Λ_n calculated with the dynamical THDFB procedure, and for relatively close clumps with $D = 20$ fm yields values that are not constant in time. Initially, the rates remain approximately constant and are overwhelmingly due to the tunneling of the most energetic neutrons. Oscillations set in at a later stage due to wave mechanical properties such as reflections and interferences. The rates drop at some later time before they flatten out at much larger time scales when less energetic neutrons start participating in the tunneling process. As expected, the neutron transfer rate increases with decreasing separation energy S_n . The rates are smaller by at least an order of magnitude of those predicted by the WKB transmission model.

The smaller transmission rates calculated with the microscopic TDHFB model is partially due to the two-body interaction which makes a large contribution E_{int} to the total nuclear binding, (see table 1). A neutron clump is stickier due to the strong neutron-neutron interaction and the “evaporation” or tunneling to free space regions is suppressed. From table 1 we see that the contribution of the two-nucleon binding to the total energy reduces from 35 MeV/neutron to 28 MeV/neutron as the neutron number increases for $N = 20$ to $N = 160$. But the separation energy S_n has a stronger influence on the transfer during the initial stages due to the tunneling of valence neutrons.

To gain more insight we switch off the two-body interaction $v(x, x')$ at $t > 0$. Figure 2 shows the average value of $\langle \Lambda_n \rangle$ for $D = 20$ fm during the interval $t = 0 - 1000$ fm/c. The error bars represent the standard deviation of the average values. The diamonds (filled circles) are obtained solving Eqs. (1) with $v(x, x') = 0$ ($v(x, x') \neq 0$). The tunneling probability increases by a factor $\simeq 4 - 5$ when the neutron-neutron interaction is turned off. This reassures the need of a many-body calculation for the diffusion process when residual nucleon-nucleon interactions are relevant.

Pairing correlations are important in two neutron transfer reactions between nuclei (Bes & Sorensen 1969; Broglia et al. 1968). The enhancement of tunneling emerges in transparent analytical models for Cooper pairs and composite particles, as shown in Refs. (Flambaum & Zelevinsky 2005; Bertulani et al. 2007). We study the impact of pairing switching off the pairing density matrix $\kappa(x, x')$ in the TDHFB equations 1, equivalent to solving the TD-Hartree-Fock equations. The Λ_n rates are barely changed, decreasing the transfer rate by less than 3% for $N = 160$ and less than 5% for $N = 20$. Therefore, there is dominance of single neutron tunneling in the 1D model. There is no direct correlation of this process with neutron transfer in heavy-ion exchange reactions because in the later case there are two time-scales; one for the reaction time, and another for the neutron tunneling dynamics. In our model, pairing is unlikely to modify the total energy by suppressing single-neutron transfer in favor of pair transfer.

We now discuss the transfer rate dependence on the distance between the neutron clumps. The same physical properties reported above are also observed with increasing separations D . The computing time increases considerably because of exponentially smaller tunneling probabilities with increasing separation distances. This feature is displayed in Table 2 for $N = 160$ using the same parameters as in Table 1 for the initial wavefunction. The diffusion rates obtained with the TDHFB calculations are about 2-15 times smaller than the predictions based on the Gamow model.

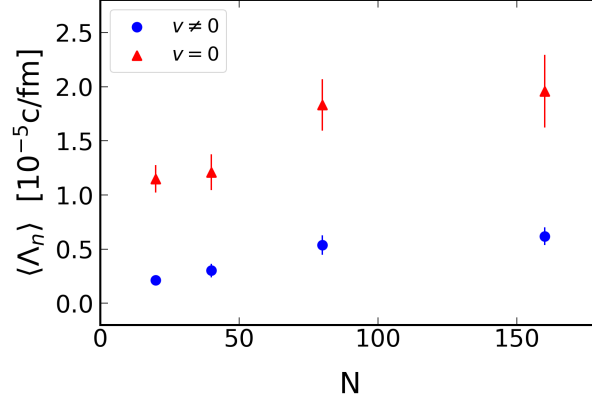


Figure 2. Average value of $\langle \Lambda_n \rangle$ for $D = 20$ fm during the interval $t = 0 - 1000$ fm/c for $N = 20, 40, 80$ and 160 . The error bars represent the standard deviation of the average values. The diamonds (filled circles) are obtained solving Eqs. (1) with the neutron-neutron interaction $v(x, x') = 0$ ($v(x, x') \neq 0$).

D	20 fm	35 fm	50 fm	100 fm
$\langle \Lambda_n \rangle$	5.16×10^{-6}	1.13×10^{-9}	2.24×10^{-12}	4.77×10^{-24}
Λ_G	9.51×10^{-6}	1.24×10^{-8}	1.35×10^{-11}	2.93×10^{-22}

Table 2. Average tunneling probabilities $\langle \Lambda_n \rangle$ (in units of c/fm) with increasing separation distances for $N = 160$ using the same parameters as in Table 1 for the initial wavefunction. The second row displays the results of the WKB method based on Eq. (10).

The transfer rates reported here are large compared to typical ones in nuclear reactions because of the large neutron numbers and small separation energies we have adopted for the valence neutrons. Because of the Coulomb barriers and symmetry energies in normal nuclei, and for large separation between them, the transfer rates are much smaller. On the other hand, as the neutron number increases in the envelope and crust of neutron stars, the reaction rates are expected to increase accordingly when inhomogeneous conditions develop. We have also considered neutron clumps with 500 and 1000 neutrons with widths and depths of the confining potentials $U(x)$ adjusted to accommodate all neutrons within the potential wells while keeping the valence neutrons at about 1 MeV binding. This time, the distance between the edges of the clumps were kept fixed at 100 fm. We obtain $\langle \Lambda_n \rangle \sim 7.23 \times 10^{-22}$ c/fm and $\langle \Lambda_n \rangle \sim 5.14 \times 10^{-20}$ c/fm for $N = 500$ and 1000 , respectively. This is in agreement with the increase of the diffusion rate with the neutron number, but it is manifestly stronger for large clumps. It is a probable scenario in a cataclysmic event, i.e., large neutron clumps separated by large distances. If the distances become smaller due to compression waves, the neutron diffusion process can release enormous amounts of energy.

4. FRBS AND MAGNETARS.

Fast radio bursts (FRBs) are a new astrophysical electromagnetic phenomenon discovered in recent years. These are radio pulses with unknown origin and the research in this field is fairly nascent. Theories to explain this phenomenon are diverse (Platts et al. 2019), ranging from highly speculative (as for example, invoking alien civilizations) to more standard ones, such as merger of compact stars (Totani 2013; Liu 2018) and fracturing crusts (Suvorov & Kokkotas 2019). The radio pulses are very bright with brief durations, typically in a range from $\sim 30 \mu\text{s}$ to ~ 20 ms (Gajjar et al. 2018; Michilli et al. 2018; Katz 2018) and apparently there is no indication of repetition for the majority of them. Relativistic particle beams with large Lorentz factors γ are possibly involved in the emission process, in a pulsar-like mechanism, where e^\pm pairs are created and accelerated to ultra-relativistic speeds in the polar cap region. Radiation coherence makes N particles radiate with N^2 times the single-particle emission (Cordes & Chatterjee 2019). In a pulsar model the spindown power is responsible for the electromagnetic radiated power, i.e., the loss of rotational energy of the star provides the power, therefore an instantaneous emission cannot exceed the spindown power in these radio emitters. However, this is possible for magnetars (SGRs/AXPs), where the radiated power is believed to come

from the huge magnetic field ($B \sim 10^{12} - 10^{15}$ G) instead of rotation, i.e., the decay of the ultra-strong magnetic field generates the emission. Unpredictable and unknown instabilities in these sources are responsible for bursting/flaring activities in X and gamma-ray spectrum from few milliseconds to tens of seconds. There are three kinds of bursts: the short ones, with $\sim 10^{39} - 10^{41}$ erg/s; the intermediates ones, with $\sim 10^{41} - 10^{43}$ erg/s; and the giant flares, which are exceptionally rare events with energies of $\sim 10^{44} - 10^{47}$ erg/s. According to the McGill (Olausen & Kaspi 2014) online catalog¹ only five of thirty sources are radio-emitters (in a quiescent state), and it seems that the origin of the radio emission in these sources is different from standard radio-pulsars (Turolla et al. 2015).

Recently, it was raised the possibility that FRBs have their origin in magnetars (Margalit & Metzger 2018), and there are some evidences showing that; polarization measurements suggest that FRBs sources are strongly magnetized, the localization of several FRBs to star-forming regions typical of magnetars (Bochenek et al. 2020b), the soft gamma-rays repeaters (SGRs) emit giants flares/bursts with volatility, and a more recently observation (Mereghetti et al. 2020) showed that X-ray bursts from the magnetar SGR 1935+2154 were also accompanied by a very bright millisecond radio burst. Several magnetohydrodynamics instabilities can occur in few seconds (Kokkotas 2014), the lack of correlation between bursts and waiting times suggests that the trigger mechanism could be small scale intrinsic (non-global) mechanism and episodic (Suvorov & Kokkotas 2019). Li et al. (2019) showed that the waiting time ($10^{-2} - 10^{-3}$) is of the order of the Alfvén crossing time

$$t_A \sim 10^{-3} \left(\frac{\rho}{10^{13} \text{ g cm}^{-3}} \right)^{1/2} \left(\frac{L}{10^5 \text{ cm}} \right) \left(\frac{B}{10^{15} \text{ G}} \right)^{-1} \text{ s}, \quad (10)$$

where ρ is the crustal density, $L \sim R_\odot - R_c$, with R_\odot being the stellar radius and R_c the crustal radius.

It was suggested that radio emission bursts might originate from the closed field zone within the near magnetosphere of the magnetar (Wadiasingh & Timokhin 2019), in a pulsar-like mechanism occurring near the surface of the star generated by a crust yielding event. Along the same lines, others mechanisms (Beloborodov 2017) have also considered a crustal/quake event (Petroff et al. 2019).

Here we propose that the trigger for the short gamma/X-ray bursts and FRBs could be the diffusion of neutrons in an inhomogeneous density environment in the crust. The diffusion can occur in a short time in a region at the crust where neutron-rich nuclei or neutron clumps donate neutrons to a neighborhood poor in neutron content, generating beta decay or gamma emission and thus releasing a large amount of energy. The electron from the beta decay is relativistic in the regions where the density is $> 10^6$ g/cm³ and will act as seeds for the high energy emission and coherent emission which leads to a brief radio emission. These electrons come out from the crust to the inner magnetosphere and will give rise to a e^\pm cascade, producing the high-energy radiation via synchrotron or inverse Compton scattering. These mechanisms will drive Alfvén waves, and as shown in Ref. (Kumar & Bošnjak 2020), a large-amplitude Alfvén wave packet is possible to be launched by a disturbance in the near surface of the magnetar and part of the wave energy is converted to coherent radio emission in few tens of the neutron star radii. Changes in the neutron density could also lead to pressure perturbations $\Delta P \sim n_e \Delta \mu$, where $\Delta \mu = \mu_e + \mu_p + \mu_n$, i.e., the pressure gradient is related to the chemical potentials. The pressure gradient leads to perturbations in the magnetic field and through ambipolar diffusion it heats up the crust (Beloborodov & Li 2016).

To provide a crude estimate of the total energy released in a burst, E_{burst} , we assume that on average the separation energy of the valence neutrons is $\epsilon \sim 1$ MeV and the ensuing tunneling to a neighboring site releases a similar amount of energy. Thus,

$$E_{\text{burst}} \equiv \epsilon N_{\text{cl}} P(\epsilon) \sim \frac{\epsilon N_{\text{cl}} \hbar}{\sqrt{2m\epsilon}} \exp \left(\frac{-2D\sqrt{2m\epsilon}}{\hbar} \right), \quad (11)$$

where we use the WKB tunneling probability $P(\epsilon)$ for a step barrier with width D and N_{cl} is the number of neutron clumps involved in the process. We further assume that the clumps have a dimension αD , where $\alpha > 1$ takes into account large clump sizes. Notice that the separation distance D is now representing the distance between the edges of the neutron clumps.

To determine the number of neutron clumps involved in a rapid emission, we consider the polar cap region, which can be estimated through the cylindrical region of radius R_L encapsulating the closed magnetic field lines. The maximum velocity of the particles within this region will be the speed of light, so that $c = \Omega R_L$, with Ω being the star rotational

¹ <http://www.physics.mcgill.ca/~pulsar/magnetar/main.html>

angular frequency. In the particle emission region, the lines are open and the boundaries define the polar cap with a radius, in the dipole field, given by $R_p = R \sin \theta_p = R \sqrt{R/R_L} = R \sqrt{\Omega R/c}$, where R is the star radius (see, e.g., Ref. (Ghosh 2007)). Therefore, the polar cap radius will depend on the period $P = 2\pi/\Omega$ (for magnetars, 2 – 12 s) and the star radius R . Considering a neutron star with $R = 11$ km, then $R_p \approx 118 - 48$ m for $P = 2$ and 12 s respectively. The polar cap in a twisted magnetic field configuration is $R_p = R \sin \theta_p = R \sqrt{(R\Omega/c)^n/(15 + 17n)/32}$, where n evolves from $n < 1$ to $n = 1$. Twisted field lines may enhance the polar cap radius in magnetars to about 1 or 2 km (Tong 2019). We can estimate the height under the polar cap, h_{ρ_0} , from the star surface to the layer of density $\rho = \rho_0$, where ρ_0 is the nuclear matter saturation density, yielding $h_{\rho_0} \gtrsim 3$ km. Thus, the volume of interest for the emission region in magnetars is $V = \pi R_p^2 h_{\rho_0}$. The number of clumps in this region is

$$N_{cl} = \frac{V}{4/3\pi(\alpha D)^3} \sim \frac{3R^2 h_{\rho_0}}{4\alpha^3 D^3} \frac{(R\Omega/c)^n}{(15 + 17n)/32}. \quad (12)$$

We consider three scenarios with $\alpha = 1, 5, 10$ and 50, taking into account neutron clumps which can also be much larger than the distance between them. In figure 3 we show the energy emitted in a burst as a function of their separation distance D , considering a polar cap radius $R_p = 2$ km. The green shaded horizontal region displays the observed values of short bursts in magnetars $\sim 10^{39} - 10^{41}$ erg/s (Turolla et al. 2015) and the shaded orange, the values of FRBs $\sim 10^{38} - 10^{46}$ erg/s (Zhang 2020).

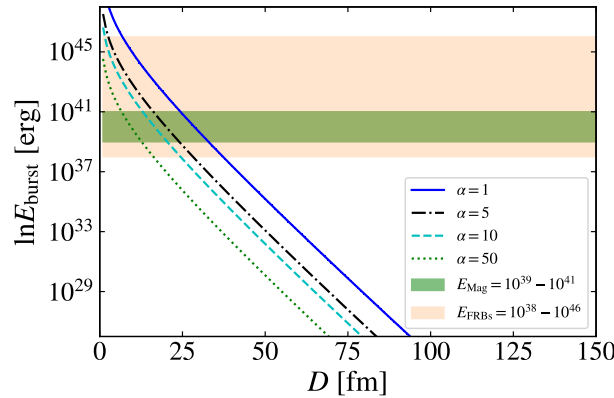


Figure 3. Energy burst as function of the separation distance D for $\alpha = 1, 5, 10, 50$. The green shaded horizontal region represents the observed values of short burst in magnetars, while the orange represents the observed values of FRBs.

Figure 3 also shows that the bursts can become comparable with the observed values of short burst in magnetars, and the observed values of FRBs, if the dense neutron sites are within distances of $D \sim 35$ fm, or below. These are rough estimates based on the WKB approximation with possible corrections by at least an order of magnitude. As we have discussed previously, a microscopic calculation can change these results appreciably if carried out within a proper three-dimensional lattice which offers more tunneling opportunities. One also sees from the figure that smaller neutron clumps favor larger energy yields. This feature is likely to remain as a robust result in more detailed microscopic calculations.

5. CONCLUSIONS

We have developed a microscopic TDHFB model to describe neutron diffusion rates due to tunneling from “neutron clumps” to regions voided of neutrons. The model is one dimensional but displays many features of the time dependent behavior of strong interacting particles.

Our main findings in this study include, but are not limited to: (a) There are marked differences between estimates based on WKB models and the time-dependent microscopic modeling for the detachment and diffusion of neutrons in an inhomogeneous neutron environment. (b) Tunneling is smaller than those obtained with perturbative (i.e., WKB) predictions, but this could change in three-dimensional calculations. (c) The role of pairing is subtle and might strongly depend on the system being studied.

Time-dependent microscopic calculations show that the subject of density homogenization and isospin diffusion in nuclear reactions and in stellar environments deserves more extensive studies. Perturbative estimates are likely to yield poor results because of the microscopic properties of strongly interacting systems such as the different contributions of the interactions to the total energy and the related energy rearrangement due to tunneling. Microscopic calculations are rich in physics details and are now becoming feasible for 3D calculations, e.g. Ref. (Stetcu et al. 2015) with the shortcoming of costly computation time even with supercomputers.

Perturbations within cataclysmic environments such as supernovae, neutron star mergers, or the creation of inhomogeneous regions in the crust of neutron stars due to compression waves from a star quake, can all lead to gamma or radio bursts when proper conditions for neutron diffusion is attained. Nuclear physics dictates that such conditions depend on the existence of inhomogeneous neutron matter clumps separated by relatively small distances.

ACKNOWLEDGEMENTS

We have benefited from useful discussions with Sanjay Reddy and Takashi Nakatsukasa. This work has been supported in part by the U.S. DOE Grant No. DE-FG02-08ER41533.

REFERENCES

- Andersen, B. C., Bandura, K. M., Bhardwaj, M., et al. 2020, *Nature*, 587, 54
- Beloborodov, A. M. 2017, *The Astrophysical Journal*, 843, L26
- Beloborodov, A. M., & Li, X. 2016, *Astrophysical Journal*, 1
- Bertulani, C. A., Flambaum, V. V., & Zelevinsky, V. G. 2007, *Journal of Physics G: Nuclear and Particle Physics*, 34, 2289
- Bes, D. R., & Sorensen, R. A. 1969, *The Pairing-Plus-Quadrupole Model* (New York, NY: Springer US), 129–222
- Bochenek, C. D., Ravi, V., Belov, K. V., et al. 2020a, *Nature*, 587, 59
- Bochenek, C. D., Ravi, V., & Dong, D. 2020b, *arXiv:2009.13030 [astro-ph]*, *arXiv:2009.13030*
- Brogia, R. A., Riedel, C., & Soerensen, B. 1968, *Nucl. Phys. A*, 107, doi:10.1016/0375-9474(68)90718-5
- Chugunov, A. I. 2018, *Monthly Notices of the Royal Astronomical Society: Letters*, 483, L47
- Cordes, J. M., & Chatterjee, S. 2019, *Annual Review of Astronomy and Astrophysics*, 57, 417
- Flambaum, V. V., & Zelevinsky, V. G. 2005, *Journal of Physics G: Nuclear and Particle Physics*, 31, 355
- Fryer, C. L., Herwig, F., Hungerford, A., & Timmes, F. X. 2006, *The Astrophysical Journal*, 646, L131
- Gajjar, V., Siemion, A. P. V., Price, D. C., et al. 2018, *The Astrophysical Journal*, 863, 2
- Gamow, G. 1928, *Zeitschrift für Physik*, 51, 204
- Ghosh, P. 2007, *Rotation and Accretion Powered Pulsars* (World Scientific)
- Katz, J. I. 2018, *Progress in Particle and Nuclear Physics*, 103, 1
- Kokkotas, K. D. 2014, *AIP Conference Proceedings*, 1577, 119
- Kumar, P., & Bošnjak, Ž. 2020, *Monthly Notices of the Royal Astronomical Society*, 494, 2385
- Li, B., Li, L.-B., Zhang, Z.-B., et al. 2019, *International Journal of Cosmology, Astronomy and Astrophysics*, 1, 22
- Lin, L., Zhang, C. F., Wang, P., et al. 2020, *Nature*, 587, 63
- Liu, X. 2018, *Astrophysics and Space Science*, 363, 242
- Margalit, B., & Metzger, B. D. 2018, *The Astrophysical Journal*, 868, L4
- Mereghetti, S., Savchenko, V., Ferrigno, C., et al. 2020, *The Astrophysical Journal*, 898, L29
- Metzger, B. D., Beniamini, P., & Giannios, D. 2018, *The Astrophysical Journal*, 857, 95
- Michilli, D., Seymour, A., Hessels, J. W. T., et al. 2018, *Nature*, 553, 182
- Ogata, K., & Bertulani, C. A. 2020, *Journal of Physics G: Nuclear and Particle Physics*, 47, 095101
- Olausen, S. A., & Kaspi, V. M. 2014, *The Astrophysical Journal Supplement Series*, 212, 6
- Petroff, E., Hessels, J. W. T., & Lorimer, D. R. 2019, *The Astronomy and Astrophysics Review*, 27, 4
- Piro, A. L., & Ott, C. D. 2011, *The Astrophysical Journal*, 736, 108
- Platts, E., Weltman, A., Walters, A., et al. 2019, *Physics Reports*, 821, 1
- Ring, P., & Schuck, P. 1980, *The nuclear many-body problem* (New York: Springer-Verlag), doi:10.1063/1.2915762
- Shi, L., & Danielewicz, P. 2003, *Phys. Rev. C*, 68, 064604
- Stetcu, I., Bertulani, C. A., Bulgac, A., Magierski, P., & Roche, K. J. 2015, *Phys. Rev. Lett.*, 114, 012701
- Suvorov, A. G., & Kokkotas, K. D. 2019, *Monthly Notices of the Royal Astronomical Society*, 488, 5887

- Tong, H. 2019, Monthly Notices of the Royal Astronomical Society, 489, 3769
- Totani, T. 2013, Publications of the Astronomical Society of Japan, 65, L12
- Tsang, M. B., Liu, T. X., Shi, L., et al. 2004, Phys. Rev. Lett., 92, 062701
- Turolla, R., Zane, S., & Watts, A. L. 2015, Reports on Progress in Physics, 78, 116901
- Wadiasingh, Z., & Timokhin, A. 2019, The Astrophysical Journal, 879, 4
- Zhang, B. 2020, Nature, 587, 45